Liquid Crystals
Publication details, including instructions for authors and subscription information:
http://www.informaworld.com/smpp/title~content=t713926090

Structural changes in discotic samples during transition from crystal to discotic mesophase as revealed by electron microscopy and diffraction

I. G. Voigt-martin[a]; R. W. Garbella[a]; M. Schumacher[ab]
[a] Institut für Physikalische Chemie, Mainz, Germany [b] Institut Charles Sadron (CRM-EAHP), CNRS, Strasbourg Cédex, France

To cite this Article Voigt-martin, I. G. , Garbella, R. W. and Schumacher, M.(1994) 'Structural changes in discotic samples during transition from crystal to discotic mesophase as revealed by electron microscopy and diffraction', Liquid Crystals, 17: 6, 775 — 801
To link to this Article: DOI: 10.1080/02678299408035472
URL: http://dx.doi.org/10.1080/02678299408035472

LIQUID CRYSTALS, 1994, VOL. 17, NO. 6, 775–801

Structural changes in discotic samples during transition from crystal to discotic mesophase as revealed by electron microscopy and diffraction

by I. G. VOIGT-MARTIN*, R. W. GARBELLA
and M. SCHUMACHER†
Institut für Physikalische Chemie, Welder Weg 11,
55099 Mainz, Germany

(*Received 29 November 1993; accepted 7 April 1994*)

Classical methods of structural analysis cannot be applied to liquid crystals because higher order reflections disappear during the transition from crystal to liquid crystal due to the reduction in long range orientational and translational correlations. However, in order to relate physical properties to the molecular architecture, it is essential to have information about molecular positions and orientations in the crystalline state as well as in the liquid crystalline state. In this work, the transition from crystalline to liquid crystalline phase is carefully monitored and the relationship between the original lattice and the new molecular positions found using electron diffraction. In addition to this, a new high resolution electron-microscopic technique is described in which the positions of molecules in the crystalline and the quenched discotic phase are directly imaged and the defects observed in the crystalline and LC phase compared and quantitatively analysed.

1. Introduction

Discotic liquid crystalline films have recently been shown to have photoconducting properties [1], while the same molecules in the crystalline phase are non-conducting. In order to understand the origin of this effect, information is required about molecular conformation and mutual orientation, as well as molecular distances involved. Unfortunately standard crystallographic procedures cannot be applied to solve the structure of liquid crystals, because the transition into the discotic phase is accompanied by a dramatic loss of high order reflections. Therefore the chosen procedure was first to examine the samples in the crystalline phase both by electron diffraction and high resolution imaging. From this information, atomic positions can be obtained and their effect on individual reflections in the highly ordered phase determined. The samples are then heated into the discotic phase. By noting the changing reflection intensities it is possible to relate these to specific molecular reorientations.

In order to obtain images, polymeric samples were quenched into the glassy phase, thus retaining their LC structure (as judged by electron diffraction), but now in a state permitting high resolution imaging. Although both X-ray and electron diffraction patterns from the discotic phase only give very limited information about the structure (intercolumnar distances), the electron images reveal details about molecular orientation, relative positions of molecules and defects in structure.

* Author for correspondence
† Present address: Institut Charles Sadron (CRM-EAHP), CNRS, 6, rue Boussingault, 67083 Strasbourg Cédex, France.

0267–8292/94 $10·00

2. Experimental

The ideal procedure would be to monitor the whole process on the same sample. Unfortunately monomeric samples, which crystallize, cannot be quenched into the glassy LC state and polymeric samples, which can be quenched into the glassy liquid crystalline phase, do not crystallize. Therefore the method used here was to choose specific discotic molecules, both in the monomeric state and attached to a polymer chain. It was ascertained that the high temperature discotic monomer and the glassy discotic polymer produced the same electron diffraction patterns. It was then possible to determine the crystal structure from the electron diffraction pattern and the high resolution images of the monomers. The monomers were heated into the LC phase in the heating stage of the microscope and their electron diffraction pattern recorded at extremely low electron doses and compared with that of the quenched polymeric phase. If they were identical, high resolution images were than obtained from the quenched polymeric phase.

2.1. *Electron microscopy*

The electron beam sensitivity of organic materials with aliphatic chains is a well known problem which has been discussed at great length by many authors for many years [2]. This problem has, without a doubt, represented a serious handicap in making a real advance in developing methods of structural analysis for organic molecules from electron diffraction data. However the enormous advances which have been made in the field of X-ray crystallography during the past two decades based on direct phase methods [3] have made improvements in the standard of electron crystallography mandatory. Fortunately, considerable progress has now been made in electron crystallography using direct phase methods [4–6]. More recently the maximum entropy approach has been developed for X-rays [7, 8] and applied to electron diffraction analysis [9, 10]. However, both of these methods require previous information about the space group as well as the intensities of a large number of reflections. This is frequently impossible for polymeric materials, so that another approach, which will be described in the following text, has to be adopted. The electron diffraction pattern was obtained in several zones by suitable orientation techniques (epitaxy, electric or magnetic field, mechanical shear) and by tilting about specific crystallographic axes. In this way, it was possible to obtain the unit cell constants. The reflections were recorded on emulsion and the intensities were quantified using a CCD camera or a densitometer. Because beam damage and dynamical scattering falsifies the intensities, appropriate precautions must be taken. Experimentally cryo- and low dose methods reduce beam damage, and dynamical scattering effects must be appropriately calculated [11, 12].

It is then necessary to place the molecule into the unit cell such that the calculated intensities correspond to those observed. The procedure for simulating the diffraction pattern was to calculate an initial conformation of the molecule, as a first approximation, using semi-empirical calculations. In some cases, simple molecular mechanics calculations were used to initiate the calculations. Subsequently, the molecule was optimized with respect to the minimum energy conformation using a semi-empirical quantum mechanical approach (MOPAC 6.0). This molecule was placed into the experimentally determined unit cell using CERIUS 3.1, a program enabling real time rotation and movement of the molecule in the unit cell, with almost instantaneous observation of the changing diffraction pattern. A best fit was obtained and final adjustments to the conformation undertaken until the molecular conformation and its

position in the unit cell were optimized and the calculated diffraction patterns corresponded to the experimental patterns in at least three perpendicular zones. The effect of dynamical scattering can be calculated either using the Eigenstate formulation [13], the reciprocal space multi-slice method of Cowley and Moodie [14] or the real space physical optics approach of Van Dyck [15]. In this work, the two latter procedures were applied and produced identical results.

By Fourier transformation, the images were calculated as a function of specimen thickness and defocus value, and these were also compared with experimental images. At this stage it is necessary to make a decision as to the precise frequency range of the required information. Electron diffraction patterns from liquid crystalline polymers always give only one or two small angle reflections, corresponding to distances in real space between 10 Å and 20 Å. Therefore it is necessary to transfer this information in the electron microscope. This requires, as we have shown previously [16], a completely different contrast transfer function to the one that is normally used in high resolution imaging. It entails the use of a specific, large, defocus value depending on the precise spatial frequencies which are to be transferred [17]. For beam sensitive organic molecules with aliphatic chains, it is impossible to defocus until an image is observed; rather, the required contrast transfer function must be calculated prior to the experiment and adjusted immediately when the sample is exposed to the beam. Alternatively, using on-line image analysis procedures, the image must be transferred directly to a computer with fast Fourier transform capabilities and the correct transfer function assessed directly from the power spectrum. Under the specific imaging conditions required for liquid crystalline glasses (low-frequency transfer), details of the shape of the molecule cannot be observed. However, the positions of the molecules and defects in translational order are made visible. We have shown elsewhere theoretically that, under these specific imaging conditions, the image contrast is proportional to the average projected potential distribution in the object, on condition that the thickness d of the sample does not exceed $410/Z$(Å) where Z is the atomic number [11].

The experimental image was then compared with the calculated image taking account of the transfer function (which gives rise to a q-dependent phase shift, depending on the defocus value) and dynamical scattering, giving rise to a phase and amplitude shift depending on sample thickness [11, 12]. The most recent versions of CERIUS can perform these calculations, based on the multi-slice formalism [13]. In the present work the calculations were performed using both the real space physical optics approach of Van Dyck [15] and the reciprocal space multi-slice approach first proposed by Cowley [14].

2.2. *Sample description*

It is well established that a large number of compounds composed of disc-like molecules have stable thermotropic liquid crystalline phases [18–23]. Furthermore, X-ray analysis of well-oriented monodomain samples obtained by preparing freely suspended liquid crystal strands about 200 μm in diameter revealed different crystallographic space groups, depending on the precise chemical constitution [21, 24, 25]. It is now established that not only do flat, disc-like molecules form discotic mesophases, but also pyramid shaped, conical and even elongated molecules. For this reason disc-like molecules with different conformations (a triphenylene ether [26, 27], a triphenylene ester [28] and a more elongated molecule (a derivative of rufigallol) [29] were chosen for this investigation. Although there is a tendency towards a hexagonal P6 2/m2/m or monoclinic $P2_1/a$ space group, each individual sample has to be evaluated

separately. For the samples in question, it will be shown that the structure is dramatically changed if an ester group, with its double-bonded oxygen, is placed in the side chains of the triphenylene ether.

For this investigation the following samples were chosen:

Triphenylene ether [26, 27]

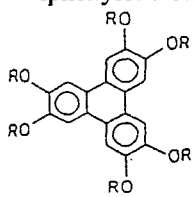

$R = C_7H_{15}$

C 64°C D 89°C I

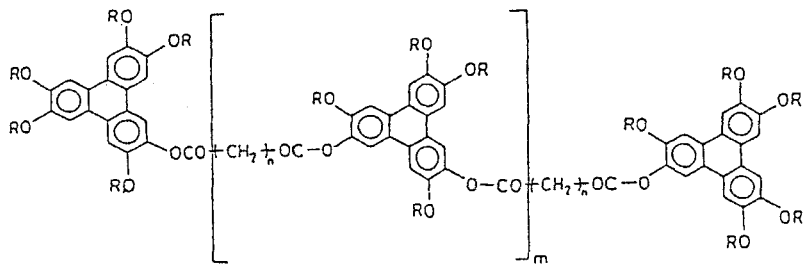

$R = -C_7H_{15}$
$m = 14$
$n = 14$

g 47°C D 182°C I

Triphenylene ester [28]

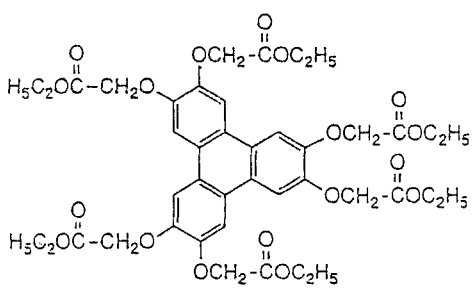

C 122°C D 172°C I

Rufigallol [29]

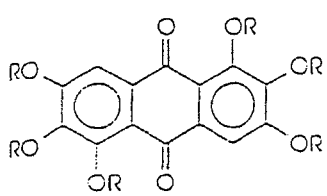

$R = C_8H_{17}$

C 0°C I 19°C II 37°C III 95·5°C I

II and III: discotic phases

2.3. *Electron diffraction*

In order to understand the structure of liquid crystals, correlation functions $G(r)$, describing the positional correlation between discotic columns or smectic layers, must be used. For perfect crystals with three dimensional long range order, $G(r)$ is a constant and its Fourier transform, the scattering function $S(q)$ consists of a series of δ-functions $S(q - q_0)$. In contrast to this, for liquids, the relevant correlation function $G(r)$ decays to zero exponentially as $\exp(-r/\xi)$, where x is the correlation length. Its Fourier transform is given by a broad lorentzian $S(q - q_0) \sim [\xi(q - q_0)^2 + 1]^{-1}$. In discotic and smectic liquid crystals, an intermediate situation exists, in which quasi long range order exists and $G(r)$ decays to zero rather slowly as $r^{-\eta}$, where η is related to the elastic constants of the material [30]. The corresponding singularity for discotics is given by a scattering function $S(q)$ in directions along and perpendicular to the column axis given by $S(q) \sim K_{12} q_\perp^2 q_z^2 + K_3 q_z^4$, where K_{12} and K_3 are the elastic constants perpendicular and parallel to the column axes. Therefore sharp Bragg spots surrounded by thermally diffuse scattering should be obtained. The difference from true long range order is subtle [31] and appears only in the wings of the scattering function.

In the kinematical approximation, the electron scattering intensity distribution is given by

$$i(q) = |f(q)|^2 \cdot |D(q)|^2 \cdot Z(q) * |S(q)|^2 + N|f(q)|^2(1 - |D(q)|^2 + i(q))_{\text{def}},$$

where $f(q)$ is the structure factor of the unit cell, N is the number of unit cells, $D(q)$ is the Debye–Waller factor describing thermal vibrations, $Z(q)$ is the reciprocal lattice factor describing lattice statistics, $S(q)$ is the shape factor, and $i(q)_{\text{def}}$ is the scattering due to isolated defects. Therefore, when passing from the crystalline into the discotic phase, all the individual peaks should remain sharp. Loss of higher order reflections is caused by the multiplicative term $Z(q)$, describing lattice statistics. Information about this term can be obtained from the images.

2.4. *Electron diffraction from triphenylene crystals and liquid crystals*

2.4.1. *Triphenylene ether*

2.4.1.1. *Crystalline triphenylene ether* (monomer)

Electron diffraction patterns were obtained from crystalline thin films oriented in two perpendicular directions. Figure 1 (*a*), (*b*) show the [001] and [010] zones of the triphenylene ether crystal. Of the two orientations, the [010] zone is by far the most frequently observed, and indicates that the columns are viewed from the side. In this diffraction pattern several aspects are particularly important:

(1) The [010] zone indicates that the a and c axes are perpendicular.
(2) The odd reflections along the equator are missing, indicating a screw axis. All reflections are present on the first layer line, with a (001) reflection corresponding to 5 Å.
(3) The most intense reflections on the first layer line are the (501) and (701) reflections, indicating that the triphenylene core is probably tilted.
(4) In the [001] zone, the a and b axes are perpendicular. Since, therefore, a, b, c are perpendicular, the crystal structure of the triphenylene ether is orthorhombic. The first, most intense reflections are the (200) at 16·3 Å and the (020) spacing at 19·15 Å. The relevant indices and d-spacings are given in table 1 (*a*). The cell constants are $a = 32{\cdot}6$ Å, $b = 38{\cdot}3$ Å, c = 5 Å and $\alpha = \beta = \gamma = 90°$, with 4 molecules per unit cell.

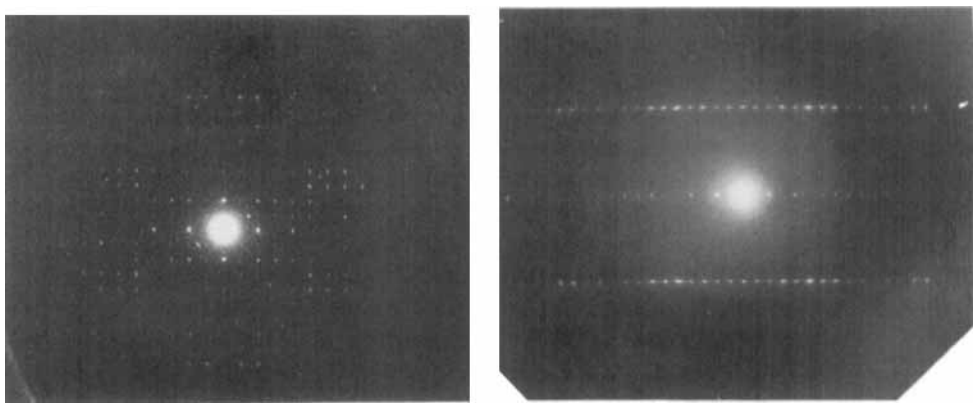

[001] zone

(*a*)

[010] zone

(*b*)

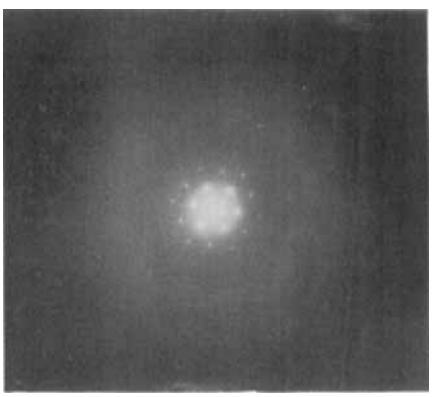

(*c*)

Figure 1. (*a*), (*b*) Discotic triphenylene ether crystal; (*c*) liquid crystal.

(5) The geometric relationship between the a and b axes is such that $a:b/2 = 1{\cdot}70$, corresponding to the geometric relationship for a hexagonal cell with a lattice constant of 19·15 Å.

2.4.1.2. *Liquid crystalline monomeric triphenylene ether*

The monomeric crystal oriented such that the [010] zone was observed (showing the discotic columns from the side) was heated into the liquid crystalline phase. The diffraction pattern changed to the hexagonal geometry as shown in figure 1 (*c*), indicating columns now viewed from the top. In this diffraction pattern the following aspects are noteworthy:

(1) The hexagonal geometry indicates complete reorientation of the molecules in the thin films during transformation into the mesophase from a [010] zone to a [001] zone.
(2) Only two orders of reflection are observed. The dramatic loss of higher order reflections is caused by loss of short range translational correlations.

Table 1 (*a*). Observed lattice spacings of triphenylene ether in the crystalline phase.

Orthorhombic unit cell:
$a = 32{\cdot}6$ Å
$b = 38{\cdot}3$ Å
$c = 5$ Å
$\alpha = \beta = \gamma = 90°$

[010] zone		[001] zone	
hkl	*d*/Å	*hkl*	*d*/Å
200	16·3	200	16·3
400	8·15	400	8·15
600	5·43	510	6·43
001	5·00	710	4·62
101	4·94	020	19·15
201	4·78	220	12·41
301	4·54	320	9·45
401	4·26	420	7·5
501	3·97	520	6·17
601	3·68	530	5·81
701	3·41	630	5·00
		730	4·38
		440	6·21
		540	5·39
		640	4·73
		740	4·19
		190	4·22
		290	4·12

Table 1 (*b*). Observed spacings of triphenylene ether momomer in the LC phase.

Hexagonal cell:	$a = b = 22{\cdot}6$ Å $\alpha = \beta = 90°$, $\gamma = 120°$
Equivalent orthorhombic cell:	$a = 22{\cdot}6$ Å $b = 39{\cdot}2$ Å

Table 1 (*c*). Observed spacings of triphenylene ether polymer in the quenched LC phase.

Hexagonal cell:	$a = b = 23{\cdot}0$ Å $\alpha = \beta = 90°$, $\gamma = 120°$
Equivalent orthorhombic cell:	$a = 23{\cdot}0$ Å $b = 39{\cdot}8$ Å

(3) The observed low order reflections are very sharp. This shows that there is quasi long range translational order in the discotic liquid crystalline phase.
(4) On cooling the sample in the electron microscope, the crystalline [010] zone reappears. The process is entirely reversible.
(5) The observed hexagonal lattice spacing is 19·6 Å, corresponding to a distance of 22·6 Å, between hexagonally arranged columns (see table 1 (*b*)). The

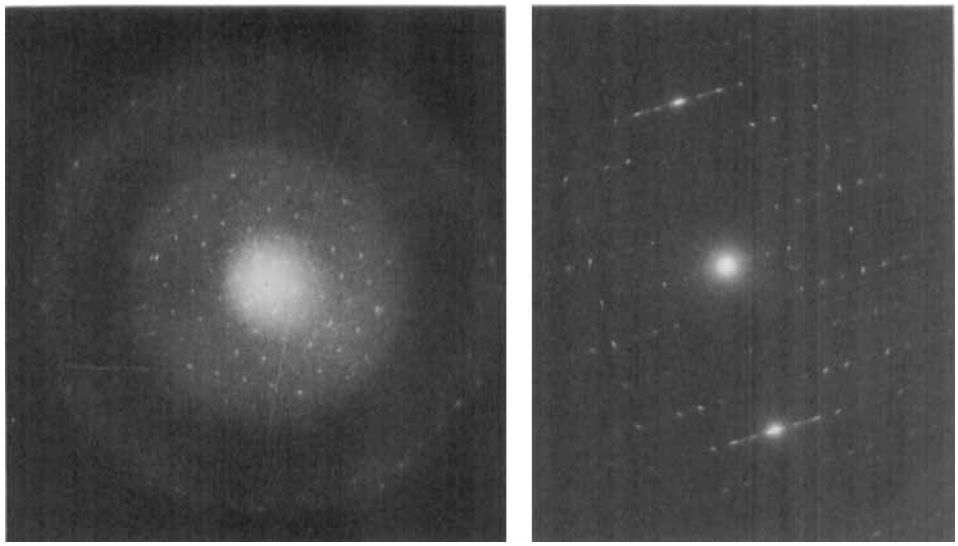

[001] zone

(*a*)

[100] zone

(*b*)

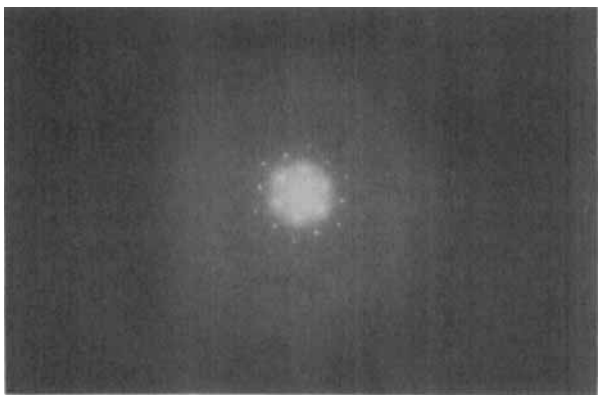

(*c*)

Figure 2. (*a*), (*b*) Discotic triphenylene ester crystal; (*c*) liquid crystal.

observed spacing of 19·6 Å is only slightly larger than the (020) spacings of the orthorhombic crystalline monomer.

2.4.1.3. *Liquid crystalline polymeric triphenylene ether glass*

The polymeric triphenylene ether does not crystallize at all, but can be quenched from the discotic mesophase into the hexagonal glassy state. The diffraction pattern from the glass is qualitatively identical to that obtained from the monomer in the LC phase and the lattice spacing, is 19·9 Å, corresponding to a spacing between the hexagonally arranged columns of 23 Å, only slightly larger than that of the monomer in the LC phase (see table 1 (*c*)).

Table 2 (*a*). Observed lattice spacings of triphenylene hexa-ester in the crystaline phase.

Hexagonal unit cell:	Orthorhombic unit cell (superstructure):
$a = 18{\cdot}8$ Å	$a = 32{\cdot}6$ Å
$b = 18{\cdot}8$ Å	$b = 56{\cdot}4$ Å
$c = 14{\cdot}2$ Å	$c = 14{\cdot}2$ Å
$\alpha = \beta = 90°$, $\gamma = 120°$	$\alpha = \beta = \gamma = 90°$

[001] zone (orthorhombic indexing)		[100] zone (orthorhombic indexing)	
hkl	*d*/Å	*hkl*	*d*/Å
060	9·40	004	3·55
130	16·3	020	28·2
190	6·15	024	3·52
200	16·3	040	14·1
260	8·14	044	3·44
2120	4·52	060	9·40
330	9·4	061	7·84
400	8·14	063	4·23
460	6·15	0120	4·70
4120	4·07		
530	6·15		
590	4·52		
660	4·70		
730	4·52		
800	4·07		

Table 2 (*b*). Observed spacings of triphenylene ester monomer in LC phase.

Hexagonal cell:	$a = b = 19{\cdot}05$ Å $\alpha = \beta = 90°$, $\gamma = 120°$
Equivalent orthorhombic cell:	$a = 32{\cdot}96$ Å $b = 19{\cdot}05$ Å

The sharp nature of the reflections is remarkable for polymers. The result indicates that the triphenylene cores assemble independently of the polymeric chains, which are situated between the columns, causing slight expansion of the lattice, but not disturbing the order of the mesogenic groups.

2.4.2. *Triphenylene ester*

2.4.2.1. *Crystalline triphenylene ester (monomer)*

In contrast to the triphenylene ether, the most commonly obtained diffraction pattern from the triphenylene ester crystal was a hexagonal [001] zone with many orders of reflection showing the columns viewed from the top (see figure 2). The perpendicular [100] zone can be obtained by shearing the sample.

(1) The [001] zone has a remarkable ring of extinctions beyond the fifth order, which is followed by a ring of reflections beginning with the tenth order (see table 2 (*a*)).
(2) The [100] zone indicates that the first strong reflection in the c^* direction is (004) corresponding to 3·55 Å. This is the closest distance between triphenylene

cores arranged horizontally (i.e. not tilted). The fact that this is a higher order reflection is shown by the superstructure reflections corresponding to 14·2 Å in the c^* direction, which is perpendicular to b^* (see table 2 (*a*)). This makes a helical arrangement of monomer units very likely.

(3) The reflection corresponding to 56·4 Å is a third order reflection. This shows that there is also a superstructure in the *b*-direction arising from the helical arrangement of the columns already observed in the [100] zone. Therefore the helices are rotated in opposing directions with a repeat every third column. The (200) reflection corresponds to a spacing of 16·3 Å. Using orthorhombic indexing to make comparison with the triphenylene ether more obvious, the unit cell is then $b = 56{\cdot}4$ Å, $a = 32{\cdot}6$ Å and $c = 14{\cdot}2$ Å. For density reasons, this requires a total of 24 molecules per unit cell.

2.4.2.2. *Liquid crystalline triphenylene ester*

On heating into the liquid crystalline phase, the transition is not easily thermally reversible, as in the triphenylene ether, but kinetically controlled. Two diffraction patterns are observed (see figure 3). In view of the preceding information, it is now easy to identify these as the [001] and [100] zones observed previously (table 2 (*b*)). The small angle reflection in figure 3 ([100] zone) corresponds to 16·5 Å, which is only slightly larger than the (200) *d*-spacing observed in the crystalline phase. The first layer line now corresponds to 3·55 Å and is arced. The additional superstructure reflections on the c^* axis are now missing.

2.4.3. *Rufigallol ether*

2.4.3.1. *Crystalline Rufigallol ether*

In the crystalline phase it was possible to obtain two different zones from the Rufigallol ether. Because of the small size of the individual crystalline grains, the diffraction spots in the [001] zone (see figure 4 (*a*)) had extended into arcs, so that the unit cell could not be determined definitely, but the measured *d*-values of the Debye–Scherrer rings did not indicate a relationship of 1·73 between planes. This therefore excludes a hexagonal unit cell. The [001] zone shows a strong reflection corresponding to 20·95 Å. On the basis of X-ray measurements, M. Werth [29] proposed an orthorhombic unit cell with $a = 30{\cdot}49$, $b = 28{\cdot}36$, in which case the reflection with a *d*-spacing of 20·95 Å would be (110). Figure 4 (*b*) show that the fourth layer line has a spacing of 3·4 Å, corresponding to the distance between Rufigallol ether molecules within a column. The diffraction pattern of figure 4 (*b*) shows that the $d = 20{\cdot}9$ Å maximum is a second order reflection and should therefore be indexed as (220). Therefore there is a superstructure in the *a*, *b*-plane and the lattice constants should be twice as large, with $a = 60{\cdot}98$ Å and $b = 56{\cdot}72$ Å. Consistent indexing of the reflections can then be obtained as indicated in table 3.

2.4.3.2. *Liquid crystalline Rufigallol ether*

On subjecting the crystalline Rufigallol ether to a higher temperature and bringing it into the liquid crystalline phase (phase III, above 37°C), a hexagonal diffraction pattern with only two very sharp orders of reflection is observed (see figure 4 (*c*)). The lattice constant is 23·2 Å. All superstructure information is missing, indicating that the molecules have lost mutual correlations between columns, while, however, retaining the intercolumnar spacing and quasi long range order. As the molecule itself has twofold

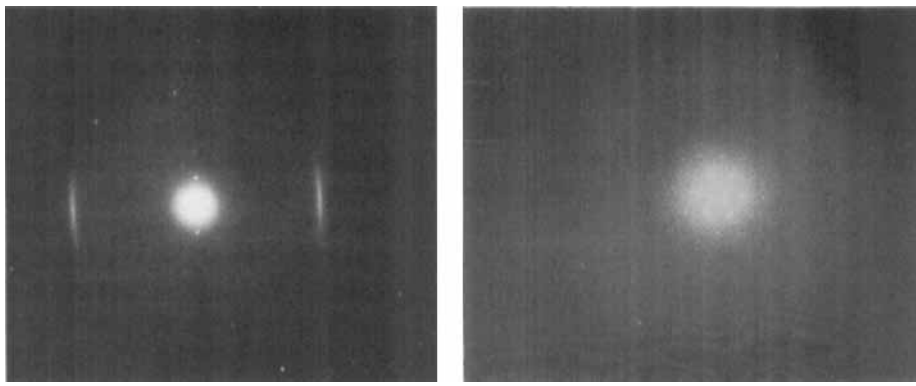

[100] zone [001] zone

Figure 3. Electron diffraction pattern from discotic triphenylenes.

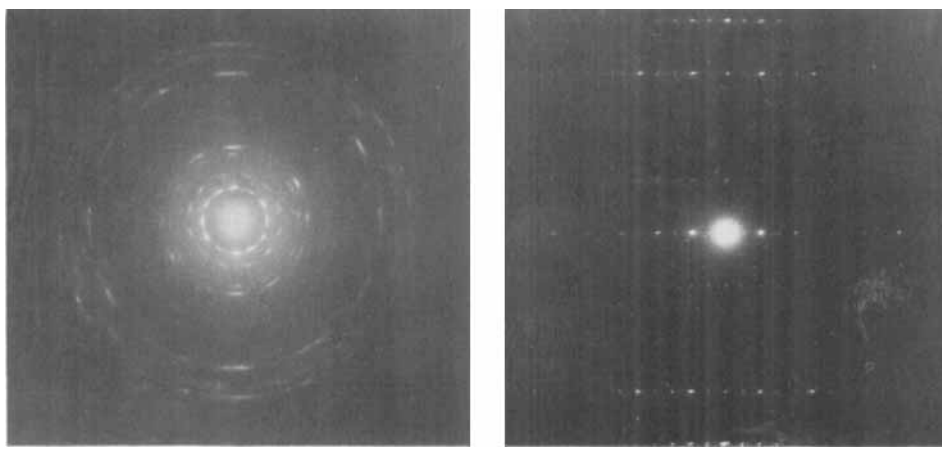

[001] zone
(*a*)

[110] zone
(*b*)

(*c*)

Figure 4. (*a*), (*b*) Rufigallol ether crystal; (*c*) liquid crystal.

Table 3 (*a*). Observed lattice spacings of Rufigallol ether in the crystalline phase (indexing based on structure proposed by M. Werth [29]).

Monoclinic unit cell:
$a = 60{\cdot}98$ Å
$b = 56{\cdot}72$ Å
$c = 13{\cdot}6$ Å
$\alpha = \beta = 90°$, $\gamma = 86°$

[001] zone		[110] zone	
hkl	*d*/Å	*hkl*	*d*/Å
220	20·95	110	41·9
400	15·1	220	20·95
440	10·6	001	13·6
		004	3·4

Table 3 (*b*). Observed spacings of Rufigallol ether in the LC phase.

Hexagonal cell:	$a = 23{\cdot}2$ Å
	$b = 23{\cdot}2$ Å
	$\alpha = \beta = 90°$, $\gamma = 120°$
Equivalent orthorhombic cell:	$a = 40{\cdot}18$ Å
	$b = 23{\cdot}2$ Å
	$\alpha = \beta = \gamma = 90°$

symmetry, the six-fold symmetry in the diffraction pattern implies rotation of the molecules in subsequent discs.

2.5. *Molecular modelling of triphenylenes*

In view of the complex nature of the molecules and the large unit cells, it is extremely difficult to simulate the diffraction patterns. For a deeper understanding of physical phenomena such as photoconductivity at a molecular level, it is however, essential to have information, not only about the architecture but also about the conformation of the molecules. This can in principle be calculated for individual small molecules using *ab initio* quantum mechanical calculations. For larger molecules *ab initio* methods become impractical and semi-empirical quantum mechanical methods must be used. They are available on public domain computer programs such as MOPAC 6.0. Clearly, the molecular conformation will be affected by the crystal field in a complex manner which will depend on details of the crystal structure and the molecules involved. Such a calculation for the large molecules in question is not possible. However, MOPAC calculations do give first estimates of the conformational features involved and are a prerequisite for structural modelling which requires simulation of the diffraction pattern. The diffraction pattern quickly indicates whether the conformation is correct or not.

A great deal of chemical knowledge is needed for molecular modelling, as well as information about similar, known structures, otherwise the calculations easily become trapped in local minima. In the cases under consideration, the lowest energy conformation of the triphenylene core is planar. However, the conformations of the side chains cause remarkable differences in the diffraction pattern.

2.5.1. *Triphenylene ether (hexaheptyloxytriphenylene)*

Several successive molecular conformations have been postulated for hexaheptyloxy triphenylene is the solid phase, arising due to 'conformational melting' of the side chains. FTIR investigations on a similar derivative showed that motion of the side chains commences at room temperature in the crystalline phase [32]. For the present investigations, the molecular conformation of the triphenylene core with a pentyloxy-side chain was calculated using MOPAC 6.0, giving the conformation shown in figure 5. The coordinates of all the molecules were stored for further use in the crystal structure simulations.

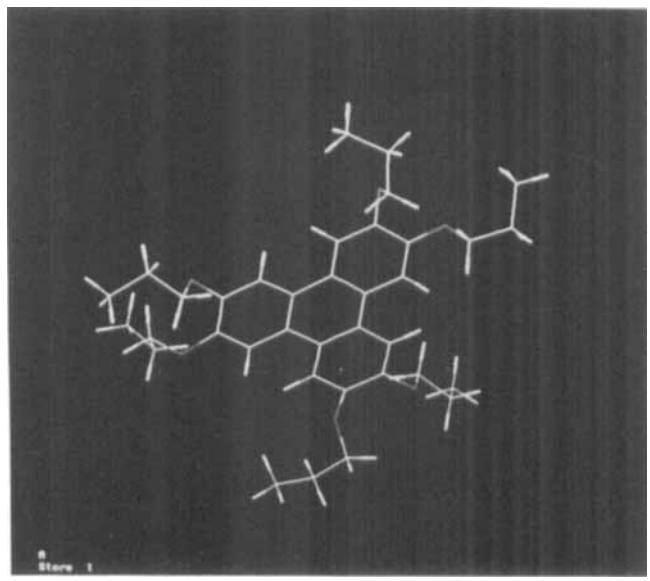

Figure 5. Conformation of triphenylene ether.

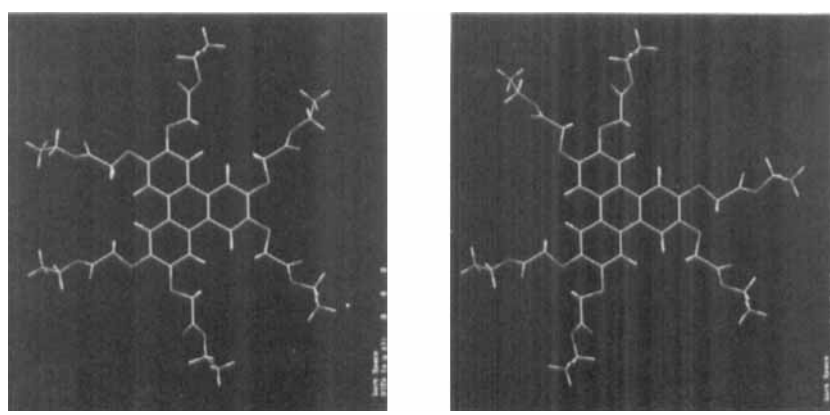

(I) (II)

Figure 6. Two possible conformations of triphenylene hexa-ester.

2.5.2. *Triphenylene hexa-ester*

The only distinguishing feature of this molecule with respect to the ether derivative is the double bonded oxygen atom. As we have shown in the experimental diffraction patterns, this has a dramatic effect on the crystal structure. In contrast to the ether group, where the single-bonded oxygen lies in the plane of the triphenylene core, the doubly bonded oxygen of the ester extends out of this plane [33–35]. The angle between the plane of the core and the carbonyl group is 56°. This angle was chosen to start the molecular simulations. Additional information about the conformation was obtained from vibrational spectra of hexa-esters of benzene [36]. For the molecule in question, two possible energy-minimized conformations were calculated (see figure 6). Good agreement with the observed diffraction pattern could be obtained only with conformation *II* which was therefore used in subsequent calculations.

2.5.3. *Rufigallol ether*

The MOPAC calculated conformation of the Rufigallol core with three carbon atoms in the side chain is shown in figure 7 (*a*). The central part of the molecule is not planar and gives a reliable minimum energy conformation. When the aliphatic chains are added to the molecule, conformation calculations become much less reliable and

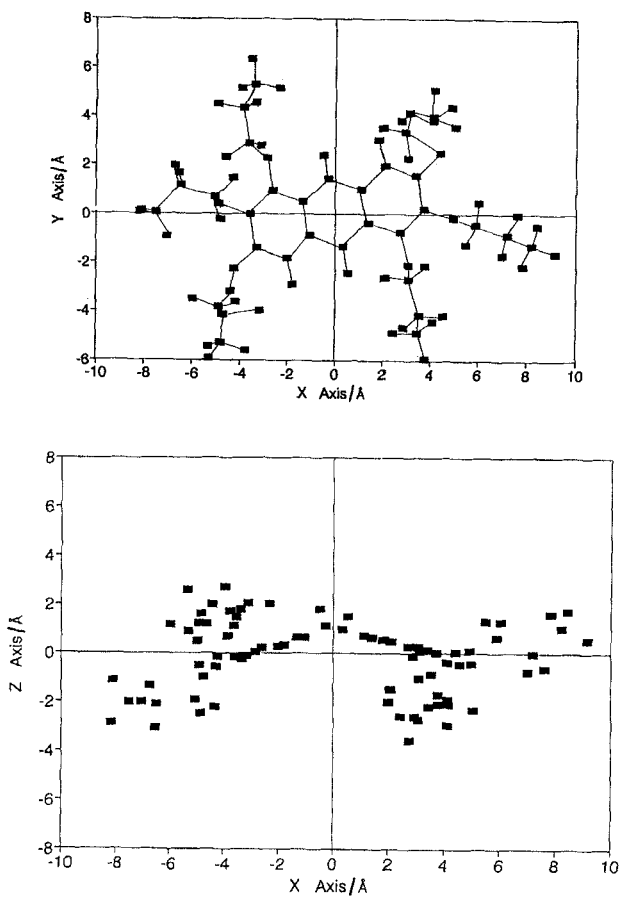

Figure 7. Conformation of Rufigallol ether molecule.

a molecule must be constructed which is capable of reproducing the experimental diffraction pattern when placed in the unit cell. Unfortunately, the crystal grains of the Rufigallol ether are so small that it was impossible to simulate the diffraction pattern adequately, so that detailed calculations corresponding to those of the triphenylenes were not possible.

2.6. *Simulation of diffraction pattern for triphenylenes*

The MOPAC calculated molecule was transferred to CERIUS, a crystallography program in which a model structure can be manipulated and the changing diffraction pattern observed in real time. For the simulations, the lattice parameters obtained from the experimental diffraction patterns are used as input, as well as a first estimation of the most likely space group as indicated by systematic absences. The initial space group is chosen on the basis of the lattice type and the observed extinctions and symmetries. Once the space group is chosen, the molecular transitions and rotations within the unit cell cannot be undertaken independently for symmetry reasons.

2.6.1. *Triphenylene ether*

By including four molecules in the unit cell with lattice parameters $a = 32{\cdot}6$ Å, $b = 38{\cdot}3$ Å, $c = 5$ Å and $\alpha = \beta = \gamma = 90°$, a density of $0{\cdot}97\,\mathrm{g\,cm^{-3}}$ was obtained. MOPAC calculations were performed for five carbon atoms in each side group. Above this, MOPAC calculations became impractical because of the large number of atoms. The strong (701) reflections indicated that the triphenylene molecule was tilted by $\pm 47°$.

Good agreement between simulated and experimental diffraction patterns for both zones was obtained for the orthorhombic model structure shown in figure 8, using the experimentally obtained cell constants $a = 32{\cdot}6$ Å, $b = 38{\cdot}3$ Å, $c = 5$ Å: $\alpha = \beta = \gamma = 90°$ and four molecules per unit cell. The molecules are tilted at $\pm 47°$ with respect to the column axis. Other tilted discotic structures in which the axial relationship is almost $\sqrt{3}$ have been described in the literature as 'pseudo-hexagonal' columnar structures [37].

2.6.2. *Triphenylene ester*

The most striking features in the experimental diffraction pattern were the additional three layer lines on the c^* axis of the [100] zone, so that the (004) reflection corresponded to the disc spacing of 3·55 Å. This gives a superstructure in the c^* direction corresponding to 14·2 Å. This is caused by a rotation of successive discs, such that every fourth disc is in register. In view of the triangular nature of the triphenylene core, there is complete overlap every 120°, so that the three additional layer lines are caused by a relative disc rotation of 30°. The best agreement with the experimental diffraction pattern in both zones was obtained by proposing a supercell with $a = 32{\cdot}6$ Å, $b = 56{\cdot}4$ Å and $c = 14{\cdot}2$ Å, $\alpha = \beta = \gamma = 90°$. This corresponds to a hexagonal arrangement of the columns, since $b/a = 1{\cdot}73$, and to hexagonal symmetry, since the six reflections have equal intensities. Because the superstructure in the b direction contains three columns, two columns are rotated in one direction, while the third rotates in the opposite direction. Similar structures have been found for triphenylene hexa-thioester [25, 38]. The model and simulated diffraction patterns in the two relevant zones are shown in figure 9.

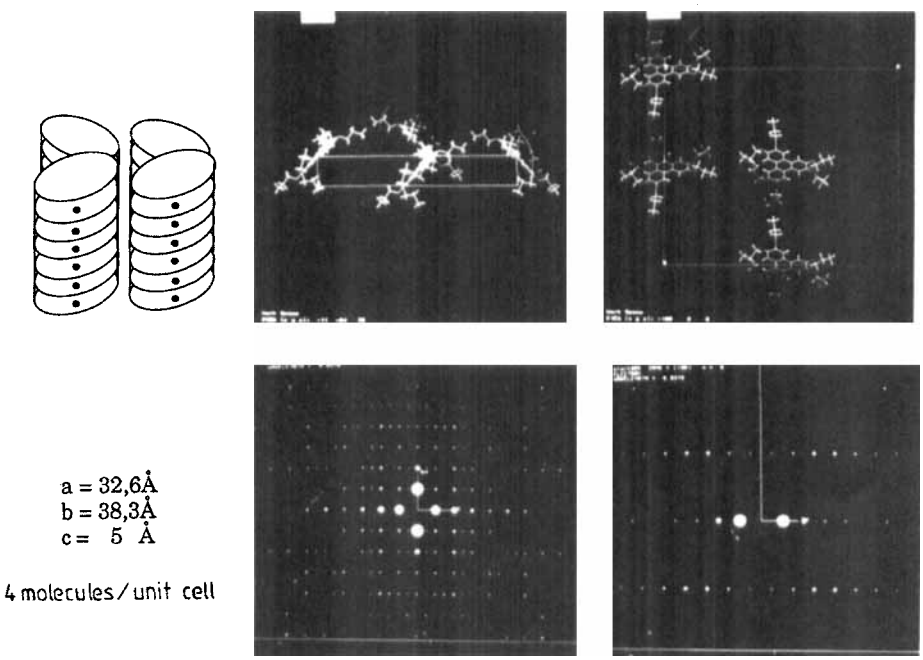

Figure 8. Structural models for triphenylene hexa-ether in crystalline phase.

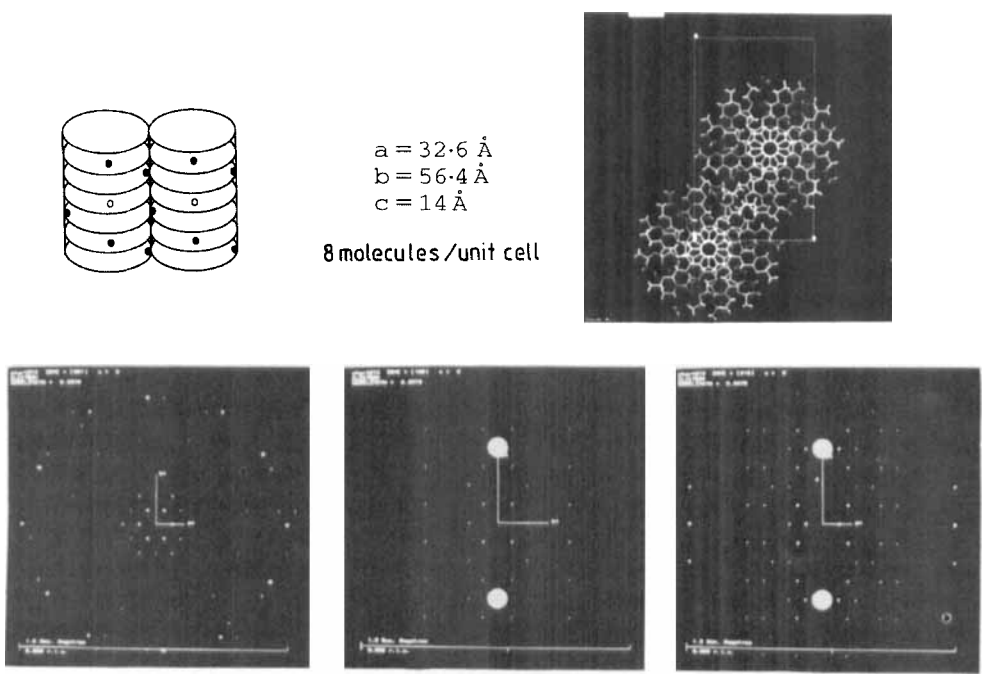

Figure 9. Structural models for triphenylene hexa-ester in crystalline phase.

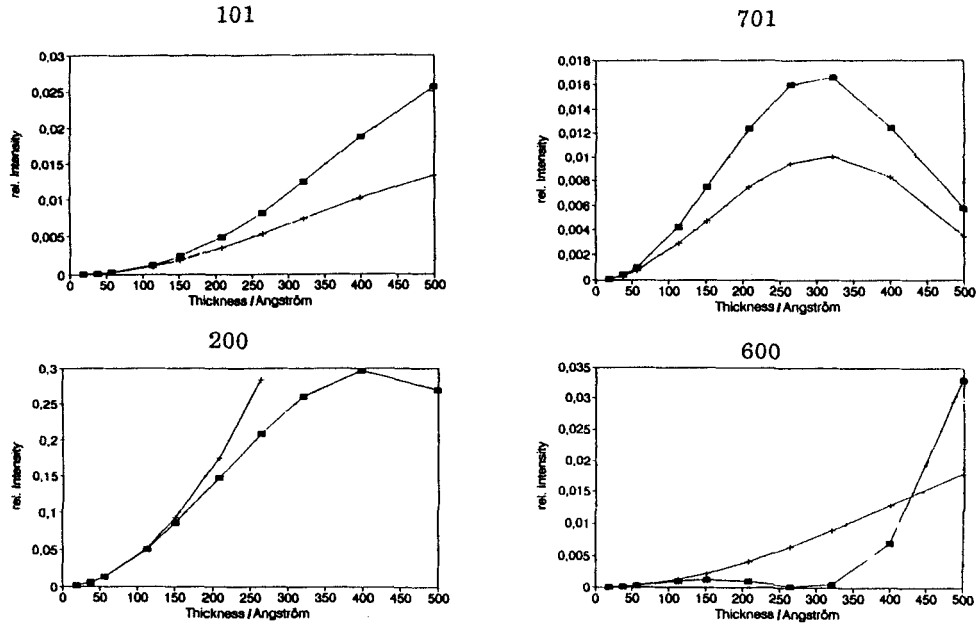

Figure 10. Effect of dynamic scattering on individual reflections. Intensity of specific triphenylene ether reflections given as a function of specimen thickness on the basis of kinematical (+) and dynamical (■) calculations.

2.7. *Effect of dynamic scattering on the diffraction pattern*

It is well known that for structure analysis and phase refinement at atomic resolution an extremely large number of independent reflections is required; about five times the number of atoms in the unit cell. For these large unit cells containing over 200 atoms per molecule this would involve over 4000 accurately measured reflections. It is clear that such a problem is easier to solve using X-rays than electrons, where it is only possible under special circumstances to obtain over 1000 reflections.

In most situations, including the one under discussion, the number of reflections obtainable is not sufficient for accurate structural analysis based on direct phase or maximum entropy methods. The only chance of doing structural analysis is then to simulate the diffraction pattern as closely as possible on the basis of a suitable model, taking account of dynamic scattering [39]. Having therefore calculated the molecular conformation, the molecule is placed into the unit cell obtained by experiment. By tilting, it is usually possible to obtain first an estimate of the space group. The molecule is manipulated in the unit cell until reasonable agreement between the experimental diffraction pattern and the diffraction pattern obtained from the model structure is obtained. Before detailed intensity comparisons are undertaken, the effect of dynamic scattering is calculated. Figure 10 shows that dynamic effects must be considered for a sample thickness above 100 Å. Unfortunately dynamic scattering events affect the intensity of each individual reflection independently, so that experimental diffraction patterns were compared with the theoretical model having the same thickness as the sample. This value was obtained by ellipsometry. The true intensities can then be obtained by calculation for samples below 100 Å.

The best agreement obtained between calculated and experimental diffraction patterns gave an R-factor of 0·34, which certainly does not correspond to a value which

an X-ray crystallographer would consider satisfactory for atomic resolution, but it is reasonable for electron crystallography, especially when intensity maxima are strongly affected by the precise conformation of the aliphatic chains attached to the discotic molecule.

Once the positions and orientations of the molecules in the crystal were understood, it was not difficult to establish the changes in position and orientation which give rise to the new diffraction pattern in the discotic phase, as will be discussed in the conclusion. However, the reason for the dramatic loss of the high order diffraction maxima could not be established until high resolution images were obtained.

2.8. *High resolution electron microscopy from crystals and liquid crystals*

Although analysis of the diffraction pattern gives vital information about the mutual relationship between the molecules and columns, this is only possible for the perfect crystal. In the liquid crystalline phase, all three substances in question have only two orders of sharp, hexagonal, small angle reflections showing the [001] zone and *d*-spacings which can easily be related to the crystalline lattice spacings. However, in order to obtain information about defects which could lead to the observed changes in photoconductivity, it was necessary to obtain medium to high resolution images. In order to do this and to interpret the micrographs correctly, the special properties of the electron microscope transfer function must be considered. We have discussed this in detail elsewhere [11].

2.8.1. *Triphenylene ether*

High resolution images were obtained from the triphenylene ether crystals both in the *ac* projection (see figure 11), showing the columns from the side, and the (rarely observed) *ab* projection (see figure 12), showing the columns from the top. The structural features have already been determined by electron diffraction and simulation. The important new major features in the images are the following: (*a*) In the *ac*-projection the columns extend for many microns and are viewed from the side (see figure 11). (*b*) In the *ab*-projection, the lattice planes are perpendicular to one another as expected for an orthorhombic structure in this projection (see figure 12). (*c*) There is an abundance of grain boundaries. (*d*) The angle between major crystallographic axes at the grain boundaries is 60°, as is to be expected because the lattice is pseudo-hexagonal. High resolution images from the quenched polymeric triphenylene ether polymer show regular hexagonal packing of the discotic columns viewed from the top (see figure 13). Careful inspection of the micrographs indicates that there are irregularities in short range order and quasi long range order. This qualitative statement will be quantified in the paragraph on correlation methods. There are no grain boundaries in the discotic phase.

2.8.2. *Triphenylene hexa-ester*

The images obtained from the triphenylene ester in the [001] zone show extremely regular hexagonal packing of the triphenylene columns viewed from the top (see figure 14).

2.8.3. *Rufigallol ether*

The images from the Rufigallol ether immediately explain the apparent increase in order in passing from the crystalline (Debye Scherrer rings) to the liquid crystalline (hexagonal single crystal diffraction pattern) phase (see figure 15). The crystalline phase

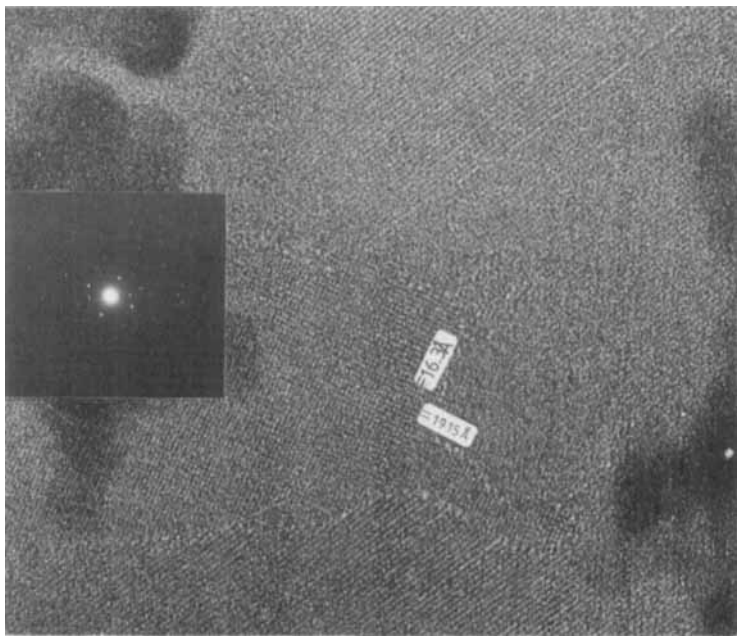

Figure 11 High resolution eletron micrograph of crystalline triphenylene ether monomer, with microdiffraction pattern in correct orientation.

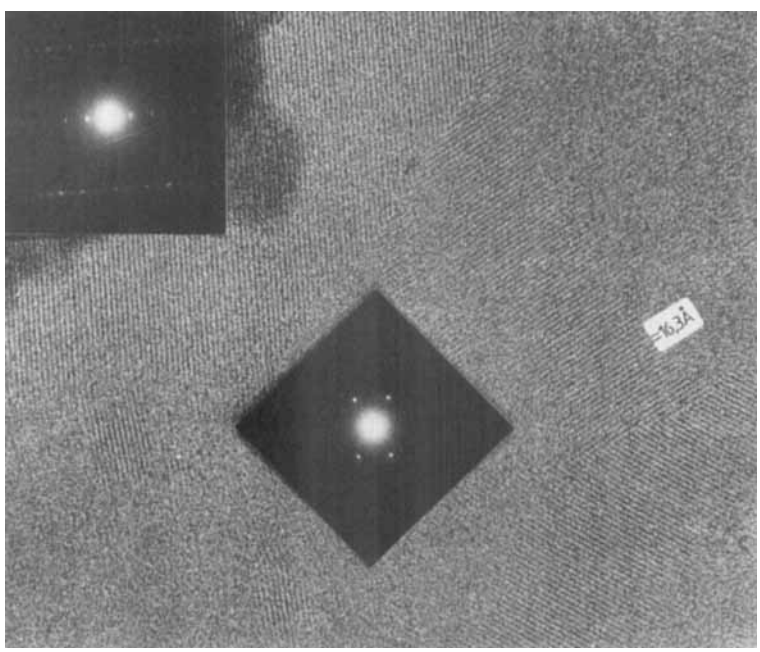

Figure 12. High resolution electron micrograph of crystalline triphenylene ether monomer, with microdiffraction pattern in correct orientation [12].

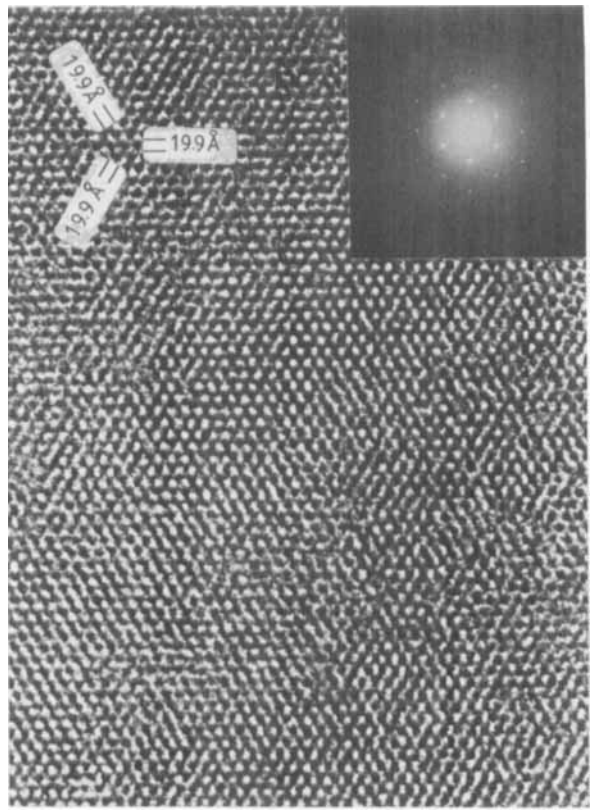

Figure 13. High resolution electron micrograph of a discotic main chain poly-ether.

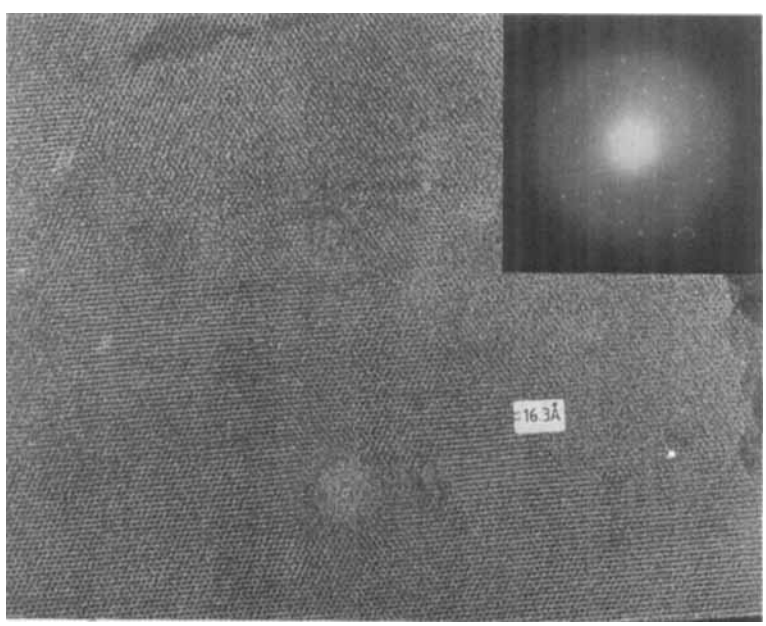

Figure 14. High resolution electron micrograph of crystalline triphenylene ester monomer, with microdiffraction pattern in correct orientation.

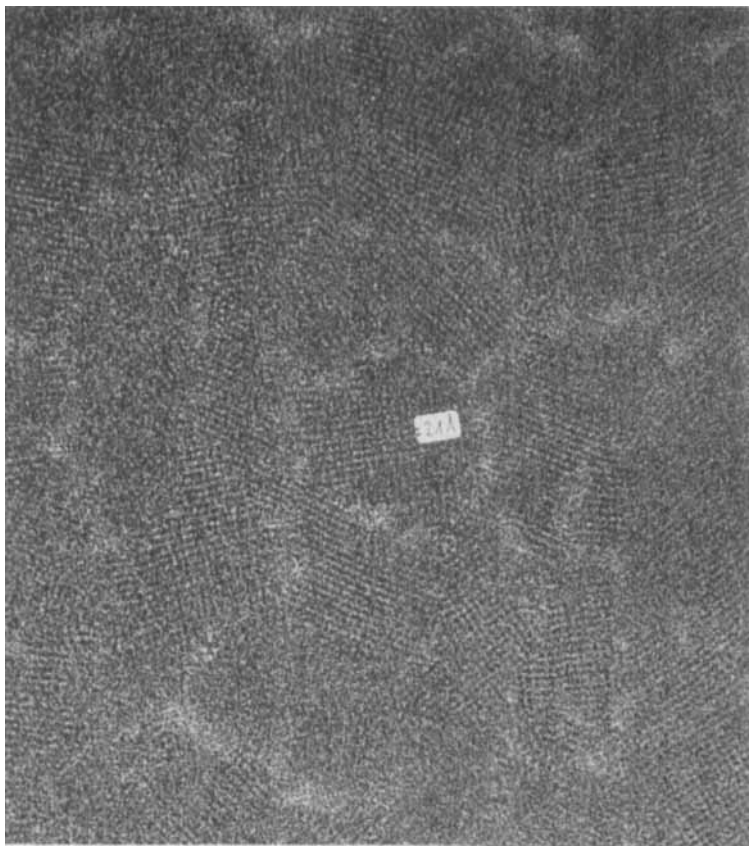

Figure 15. High resolution electron micrograph of crystalline Rufigallol in ether [001] zone.

in the *ab*-projection consists of very small grains with a diameter of only 500 Å. Within the grains, lattice planes are observed which enclose an angle of almost 90° and indicate that the structure may be monoclinic. Because of the low molecular weight of the Rufigallol ether, it was impossible to quench this material into the glassy discotic phase.

2.9. *Simulation of images and dynamic scattering effects*

An interpretation of the images observed in electron microscopy is only justified if the scattering process involved in the particular imaging technique used is fully understood and accounted for. The micrographs under discussion were obtained by a phase contrast technique, using very high defocus values of about − 5000 Å in order to transfer the low angle spatial frequencies observed in these samples. Their thickness was about 300 Å, as determined by ellipsometry. Therefore the effect of phase retardation on the image by the contrast transfer function and also due to dynamic scattering must be taken into consideration and calculated. We have used two simulation procedures, treating the convolution products both in real space [40–42] and in reciprocal space [39] for sample thickness from 100 Å to 300 Å and defocus values from − 3000 Å to − 7000 Å. The major features in the two methods are identical, while differences arise only in detail. These major features are shown in figure 16 where the results of the real space method (Van Dyck) are shown.

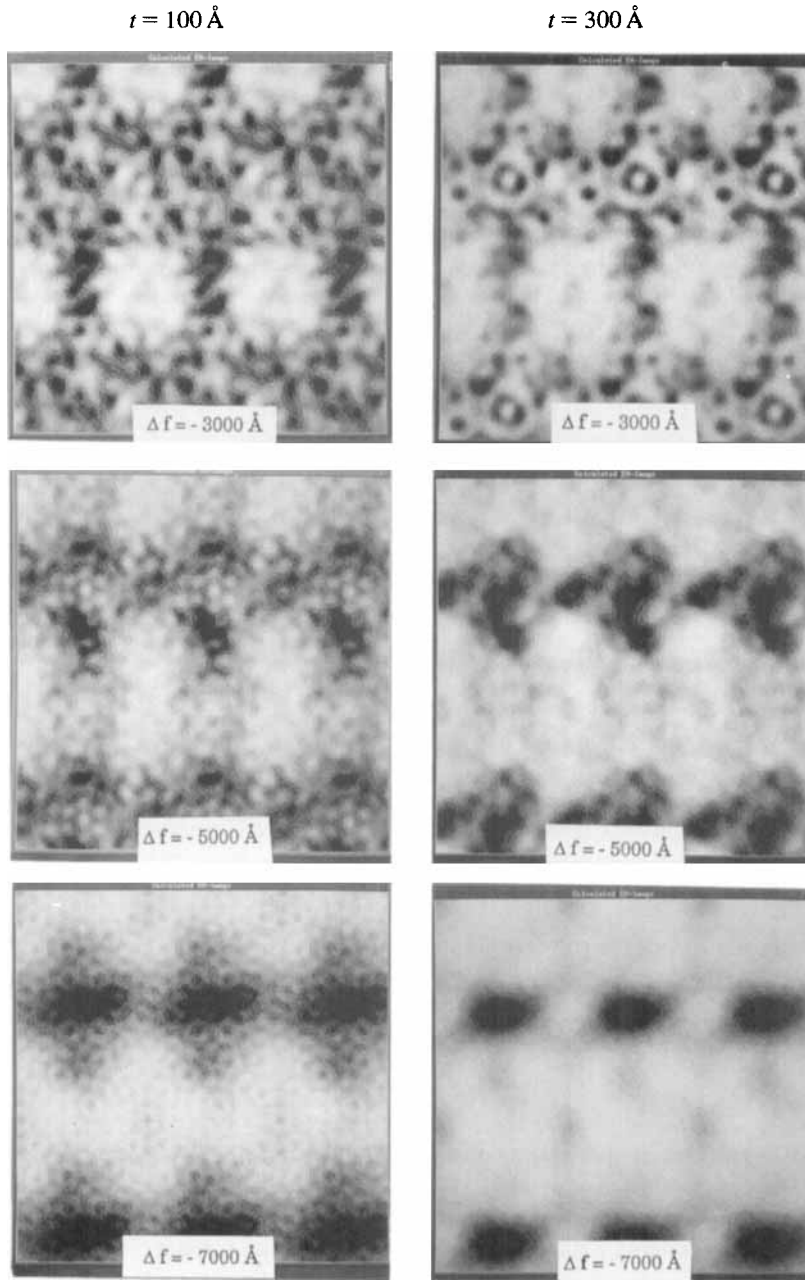

Figure 16. Effect of defocus, Δf and sample thickness, t, on image of triphenylene ether.

The calculated images demonstrate how details in the molecular structure are drastically affected by defocus value and sample thickness; even the apparent symmetry is affected. However, on approaching the region of 'low' resolution at large defocus, only the average position of the molecule is retained, while details of atomic positions are lost. However, liquid crystals are defined by correlation functions and these are

described adequately by the positions of the molecular centres which can be used to demonstrate defects such as dislocations, grain boundaries and deviations from ideal lattice positions, as experiments have shown. Since the information required for defect analysis in discotic systems involves changes in position of large molecules, medium-high resolution information is quite sufficient.

2.10. *Quantitative description of molecular deviations*

In order to describe the molecular deviations in liquid crystalline discotics two types of correlation technique were used:

(*a*) Autocorrelation function. The autocorrelation function (ACF) of a function (r) is given by

$$\rho(r) = \int f^*(r_1) f(r_1 + r)\, dr_1$$

and is a measure of a function at values of a variable differing by an amount r. We have shown elsewhere [12] that this function is, in fact, not very useful, because it only gives an average value for a correlation length, which was about 400–700 Å.

(*b*) Cross-correlation function. The cross-correlation is much more powerful, because it describes in detail the precise direction and length of the individual deviations from perfect lattice positions and this information can be obtained directly from the high resolution micrographs. In collaboration with K. Downing at Berkeley, selected areas were densitometered. The optical density measurements were truncated and packed into a dense format. The Fourier transform was calculated and a suitable mask used to filter all strong reflections. The filtered image is calculated by back-transformation and represents the perfect structure. The central area is boxed off and correlated with the true image, and vector displacements of the centres of gravity of correlation peaks from positions on the perfect lattice are plotted in figure 17, which represents a typical vector map for all discotic samples which we investigated, where the deviations have been multiplied by a factor of 10 in order to make them visible. The map shows that some deviations are directed along the axes of a hexagonal lattice, while others are rotated with respect to the lattice. There is a complete absence of grain boundaries and quasi long range order is evident. While this impression can easily be gained qualitatively directly from the micrographs, this quantitative assessment is much more satisfactory.

3. Conclusions

In the liquid crystalline phase all molecules described in this work form hexagonal columnar structures with their axes perpendicular to the film plane. This is quite extraordinary, because the individual molecules with the side chains do not all possess either threefold or sixfold symmetry. Furthermore, in the crystalline phase only the triphenylene ester forms a crystal with sixfold symmetry, whereas the triphenylene ether and the Rufigallol ether have fourfold and twofold symmetry. In the orthorhombic triphenylene ether, the lattice spacing $d_{(100)}/d_{(020)}$ is always close to 1·73, which corresponds to hexagonal geometry. Such a 'pseudo-hexagonal' arrangement has been described previously [37]. When all the lattice spacings are listed together (see table 4) the following observation is made: In order to accommodate the columns consisting of disc-like molecules, a basic orthorhombic unit is required with cell constants $a = 32{\cdot}6$ Å, $b = 18{\cdot}8$ Å, $c = 3{\cdot}4$ Å, $\alpha = \beta = \gamma = 90°$ and containing two columns/unit cell. This corresponds to a hexagonal lattice with $a = b = 18{\cdot}8$ Å; $\gamma = 120°$, $\alpha = \beta = 90°$.

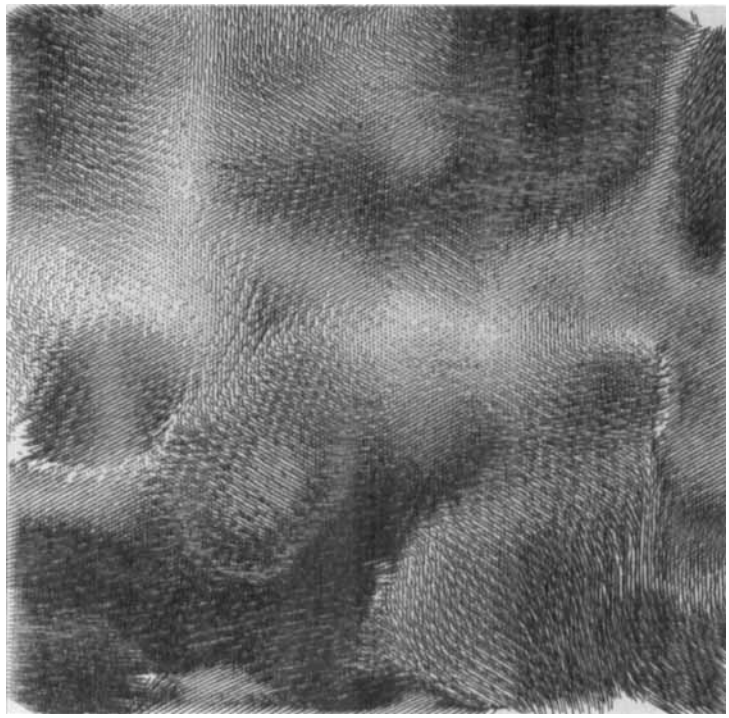

Figure 17. Deviation vectors obtained by cross-correlation of discotic 'lattice' with perfect crystal.

Simulation of the experimental diffraction patterns indicates that all the other structures for the triphenylenes can be related to multiples of this basic unit, as indicated in figure 18, with a slight expansion depending on precise molecular dimensions and temperature (see table 4). Superstructures in the *ab*-, *bc*-, and *ac*-projections arise due to tilting and helix formation.

In the discotic phase, the symmetry of individual molecules is lost due to mutual rotation of the discs about the columnar axis, making them appear circular in projection, and shifting of the columns with respect to each other. Consequently the old superstructure disappears and the basic hexagonal symmetry is seen from the top. Cross-correlation analysis of the high resolution images shows that the loss of higher order reflections arises from slight short range deviations of molecular positions from a perfect hexagonal lattice, whilst, however, quasi long range order is retained. This has been predicted theoretically [43] and found for the first time by these experiments. Over and above this, the deviation vectors shown the precise direction in which molecules are displaced from a true lattice. Figure 17 shows that the small displacements occur both in a hexagonal lattice direction and in a rotatory direction, whilst, however, quasi long range order is retained. Grain boundaries are eliminated in the discotic phase, while molecules are still close to lattice positions. The ability of these materials to act as photoconductors in the LC phase, but not in the crystalline phase, may well be related to the loss of grain boundaries. Electron diffraction is therefore a very powerful method of determining the kinds of superstructure which occur in crystals and how the transition into the liquid crystalline phase takes place.

Table 4. Relationships between basic structural units and superstructure.

	Triphenylene hexa-ether	Triphenylene hexa-ester	Rufigallol ether
Crystal hexagonal $\alpha = \beta = 90°$, $\gamma = 120°$		$a = b = 18{\cdot}8$ Å $c = 14{\cdot}2$ Å ($= 4 \times 3{\cdot}55$ Å)	
Crystal orthorhombic $\alpha = \beta = \gamma = 90°$	$a = 32{\cdot}6$ Å $b = 38{\cdot}3$ Å ($= 2 \times 19{\cdot}15$ Å) $c = 5$ Å ($= 3{\cdot}4/\cos 47°$)	$a = 32{\cdot}6$ Å $b = 56{\cdot}4$ Å ($= 3 \times 18{\cdot}8$ Å) $c = 14{\cdot}2$ Å ($= 4 \times 3{\cdot}55$ Å)	Crystal monoclinic $a = 60{\cdot}98$ Å ($= 2 \times 30{\cdot}49$ Å) $b = 56{\cdot}72$ $c = 13{\cdot}6$ Å ($= 4 \times 3{\cdot}4$ Å) $\alpha = \beta = 90°$, $\gamma = 86°$
Liquid crystal hexagonal (in *ab* plane) $\alpha = \beta = 90°$, $\gamma = 120°$	$a = b = 22{\cdot}6$ Å	$a = b = 19{\cdot}05$ Å	$a = b = 23{\cdot}2$ Å
Polymer liquid crystal hexagonal (in *ab* plane) $\alpha = \beta = 90°$, $\gamma = 120°$	$a = b = 23{\cdot}0$ Å		

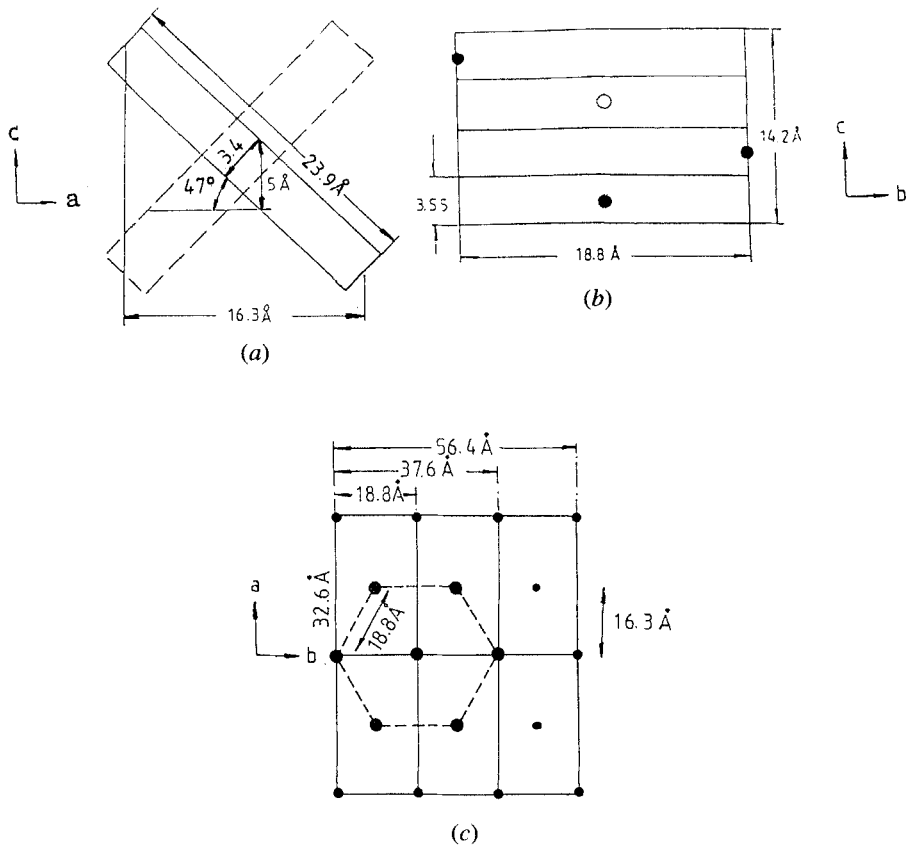

Figure 18. Origin of superstructure in triphenylenes. Relationship between molecular and lattice dimensions for triphenylene ether (*a*) in *ac* plane and triphenylene ester (*b*) in *bc* plane. (*c*) Relationship between basic unit and superstructure in *ab* plane of triphenylene hexaester in crystalline phase.

Over and above this, the images obtained by the 'medium-high' resolution technique suggested by us for liquid crystal imaging some years ago [16, 17] give invaluable information about defects, grain boundaries and dislocations in crystals, small deviations in short range order and undulations in liquid crystals. We have demonstrated that the cross-over-correlation method is powerful for this information. However, we have also shown how the diffraction pattern and high resolution images are drastically affected by dynamic scattering and the image by the contrast transfer function. In this work, we have calculated the effects of dynamic scattering, both on the diffraction patterns and on the images. The calculations show precisely how both are affected from 100 Å and above. Therefore, in these samples, the kinematic approximation must not be used for sample thicknesses greater than 100 Å.

In addition to this, the effect of the contrast transfer function on the images was calculated. We have shown elsewhere [11] that under the imaging conditions chosen here, the images represent the projected potential of the molecules, so that the deviation vectors truly represent the shift of the centres of gravity of the columns from lattice positions.

References

[1] ADAM, D., CLOSS, F., FUNHOFF, D., HAARER, I., RINGSDORF, H., SCHUMACHER, P., and SIEMENSMEYER, K.,1993, *Phys. Rev. Lett.*, **70,** 457.

[2] CREWE, A. V., ISAACSON, M. S., and ZEITLER, E., 1978, *Advances in Structure Research*, Vol. 7, edited by W. Hoppe and R. Mason (Pergamon Press).

[3] HAUTPMANN, H., 1978, *Crystal Structure Determination: The Role of the Cosine Semi-variants* (Plenum Publishing Corp.).

[4] DORSET, D., 1991, *Biophys. J.*, **60,** 1366.

[5] DORSET, D., 1986, *Macromolecules*, **19,** 2965.

[6] DORSET, D., 1992, *Ultramicroscopy*, **39,** 23.

[7] BRICOGNE, G., 1984, *Acta crystallogr.* A, **40,** 410.

[8] GILMORE, C. G., HENDERSON, A. N., and BRICOGNE, G., 1991, *Acta crystallogr.*, A, **47,** 842.

[9] DONG, W., BAIRD, T., FRYER, J. R., GILMORE, C., MACNICOL, D. D., BRICOGNE, G., SMITH, D. H., O'KEEFE, M. A., and HOVMÖLLER, S., 1992, *Nature, Lond.*, **355,** 605.

[10] VOIGT-MARTIN, I. G., YAN, D. H., and GILMORE, C., *Ultramicroscopy* (in the press).

[11] VOIGT-MARTIN, I. G., KRUG, H., and VAN DYCK, D., 1990, *J. Phys., France*, **51,** 2347.

[12] VOIGT-MARTIN, I. G., GARBELLA, R. W., and SCHUMACHER, M., 1992, *Macromolecules*, **25,** 961.

[13] LYNCH, D. F., MOODIE, A. F., and O'KEEFE, M. A., 1973, *Acta crystallogr.* A, **29,** 389.

[14] COWLEY, J. M., and MOODIE, A. F., 1957, *Acta crystallogr.*, **10,** 609.

[15] VAN DYCK, D., 1980, *J. Microscopy*, **119,** 141.

[16] VOIGT-MARTIN, I. G., and DURST, H., 1987, *Liq. Crystals*, **2,** 601.

[17] VOIGT-MARTIN, I. G., DURST, H., RECK, B., and RINGSDORF, H., 1988, *Macromolecules*, **21,** 1620.

[18] CHANDRASEKHAR, S., 1977, *Liquid Crystals* (Cambridge University Press).

[19] CHANDRASEKHAR, S., and RANGANATH, G. S., 1990, *Rep. Prog. Phys.*, **53,** 57.

[20] DESTRADE, C., FOUCHER, P., GASPAROUX, H., and TINH, N. H., 1984, *Molec. Crystals liq. Crystals*, **106,** 121.

[21] LEVELUT, A. M., 1983, *J. chem. Phys.*, **80,** 149.

[22] LEADBETTER, A. J., 1988, *Thermotropic Liquid Crystals: Critical Reports on Applied Chemistry*, Vol. 22, edited by G. W. Gray (Wiley).

[23] RINGSDORF, H., TSCHIRNER, P, HERRMANN-SCHÖNHERR, O., and WENDORFF, J. H., 1987, *Macromolek. Chem.*, **188,** 1431.

[24] FONTES, E., HEINEY, P. A., OHBA, M., HASELTINE, J. N., and SMITH III, A. B., 1988, *Phys. Rev.* A, **37,** 1329.

[25] HEINEY, P. A., FONTES, E., DE JEU, W. H., RIERA, A., CARROLL, P., and SMITH III, A. B., 1989, *J. Phys., France*, **50,** 461.

[26] KRANIG, W., 1990, Ph.D. Thesis, University of Mainz.

[27] KRANIG, W., HÜSER, B., SPIESS, H. W., KREUDER, W., RINGSDORF, H., and ZIMMERMANN, H., 1990, *Adv. Mater.*, **2,** 36.

[28] WÜSTEFELD, R., 1990, Ph.D. Thesis, University of Mainz.

[29] WERTH, M., 1992, Ph.D. Thesis, University of Mainz.

[30] CAILLÉ, A., 1972, *C. r. hebd. Séanc. Acad. Sci., Paris* B, **274,** 1418.

[31] VERTOGEN, G., and DE JEU, W. H., 1988, *Thermotropic Liquid Crystals* (Springer-Verlag).

[32] LEE, W. K., HEINEY, P. A., MCCAULEY, J. P., and SMITH III, A. B., 1991, *Molec. Crystals liq. Crystals*, **198,** 273.

[33] COTRAIT, M., MARSAU, P., DESTRADE, C., and MALTHÊTE, J., 1979, *J. Phys. Lett., Paris*, **40,** 519.

[34] PESQUER, M., COTRAIT, M., MARSAU, P., and VOLPILHAC, V., 1980, *J. Phys., Paris*, **41,** 1039.

[35] COTRAIT, M., MARSAU, P., PESQUER, M., and VOLPILHAC, V., 1982, *J. Phys., Paris*, **43,** 355.

[36] KARDAN, M., RHEINHOLD, B. B., SHAW LING HSU, RANJIT THAKUR, and LILLYA, C. P., 1986, *Macromolecules*, **19,** 616.

[37] LEVELUT, A. M., OSWALD, P., GHANEM, A., and MALTHÊTE, J., 1984, *J. Phys., Paris*, **45,** 745.

[38] FONTES, E., HEINEY, P. A., and DE JEU, W. H., 1988, *Phys. Rev. Lett.*, **61,** 1202.

[39] COWLEY, J., 1986, *Diffraction Physics* (Elsevier Science Publications).

[40] VAN DYCK, D., 1975, *Phys. Stat. Sol.* (b), **72,** 321.

[41] VAN DYCK, D., and COENE, W., 1984, *Ultramicroscopy*, **15,** 29.

[42] SPENCE, J. C. H., 1978, *Acta crystallogr.* A, **34,** 112.

[43] SELINGER, J., and BRUINSMA, R., 1991, *Phys. Rev.* A, **43,** 2910.